# Increased Coupled Gating of L-Type $Ca^{2+}$ Channels During Hypertension and Timothy Syndrome

Manuel F. Navedo, Edward P. Cheng, Can Yuan, Scott Votaw, Jeffery D. Molkentin, John D. Scott and Luis F. Santana

*Circulation Research* 2010, 106:748-756: originally published online January 28, 2010
doi: 10.1161/CIRCRESAHA.109.213363
Circulation Research is published by the American Heart Association. 7272 Greenville Avenue, Dallas, TX 72514
 Print ISSN: 0009-7330. Online ISSN: 1524-4571

# Increased Coupled Gating of L-Type $Ca^{2+}$ Channels During Hypertension and Timothy Syndrome

Manuel F. Navedo, Edward P. Cheng, Can Yuan, Scott Votaw, Jeffery D. Molkentin, John D. Scott, Luis F. Santana

**Rationale: L-Type (Cav1.2) $Ca^{2+}$ channels are critical regulators of muscle and neural function. Although Cav1.2 channel activity varies regionally, little is known about the mechanisms underlying this heterogeneity.**

**Objective: To test the hypothesis that Cav1.2 channels can gate coordinately.**

**Methods and Results: We used optical and electrophysiological approaches to record Cav1.2 channel activity in cardiac, smooth muscle, and tsA-201 cells expressing Cav1.2 channels. Consistent with our hypothesis, we found that small clusters of Cav1.2 channels can open and close in tandem. Fluorescence resonance energy transfer and electrophysiological studies suggest that this coupling of Cav1.2 channels involves transient interactions between neighboring channels via their C termini. The frequency of coupled gating events increases in hypertensive smooth muscle and in cells expressing a mutant Cav1.2 channel that causes arrhythmias and autism in humans with Timothy syndrome (LQT8).**

**Conclusions: Coupled gating of Cav1.2 channels may represent a novel mechanism for the regulation of $Ca^{2+}$ influx and excitability in neurons, cardiac, and arterial smooth muscle under physiological and pathological conditions. (*Circ Res*. 2010;106:748-756.)**

**Key Words:** Cav1.2 channels ■ PKC ■ calmodulin ■ arrhythmias

Voltage-gated L-Type (Cav1.2) $Ca^{2+}$ channels are expressed in the surface membrane of neurons and muscle cells, where they regulate multiple processes including excitability, contraction, gene expression, and memory storage.[1–4] Recent studies have revealed an unexpected feature of Cav1.2 channels: their activity (ie, open probability, $P_o$) varies within the cell membrane.[5–7] Low activity Cav1.2 channels open randomly and infrequently at rest, producing brief elevations in intracellular $Ca^{2+}$ concentration ($[Ca^{2+}]_i$) called "$Ca^{2+}$ sparklets."[8] In contrast, small clusters of Cav1.2 channels can function in a high open probability mode that generates localized zones of relatively high $Ca^{2+}$ influx ("persistent $Ca^{2+}$ sparklets").

Although targeting of protein kinase (PK)C$\alpha$ to the surface membrane by the kinase anchoring protein AKAP150 (the rodent ortholog of human AKAP79) increases the probability of persistent Cav1.2 channel activity,[9] the mechanisms by which small clusters of these channels open concertedly are unknown. Here, we used fluorescence resonance energy transfer (FRET) approaches in combination with optical and electrophysiological recordings of $Ca^{2+}$ influx via Cav1.2 channels to investigate this important issue. Our data indicate that activators of PKC$\alpha$, calmodulin (CaM) antagonists, or a specific Cav1.2 channel mutation that causes arrhythmias and autism in humans with the Timothy syndrome (TS) move the ubiquitous $Ca^{2+}$-binding protein CaM from the IQ domain in the C-terminal tail of the channel. This induces functional interactions between nearby Cav1.2 channel via their C termini that could lead to coupled gating of these channels.

## Methods

An expanded Methods section is available in the Online Data Supplement at http://circres.ahajournals.org.

### Isolation of Arterial and Adult and Neonatal Cardiac Myocytes

Mice and rats were euthanized as approved by the University of Washington Institutional Animal Care and Use Committee. Adult arterial myocytes and neonatal cardiac myocytes were prepared as described previously.[5,10]

### Cav1.2 and Calmodulin Constructs and Inducible PKC$\alpha$ Translocation System and Their Expression in tsA-201 Cells

We transfected tsA-201 cells using JetPEI (Polyplus Transfection) with plasmids encoding calcium channel pore-forming and accessory subunits as well as CaM. We generated the rabbit homolog of the human TS Cav1.2 (G436R, rabbit; G406R human).[11] Wild-type (WT) CaM and the Cav1.2 mutant with a stop codon at amino acid 1670 (Cav1.2$\Delta$1670X) were kindly provided by Dr David T. Yue (Departments of Biomedical Engineering and Neuroscience, The Johns Hopkins University, Baltimore, Md). We generated a rapamycin-induced PKC$\alpha$ translocation system similar to the one developed by Liberles et al[12] and Suh et al.[13] Reagents for this system were obtained from Agilent Technologies and Dr John Exton

Original received November 16, 2009; revision received January 11, 2010; accepted January 19, 2010.

From the Department of Physiology & Biophysics (M.F.N., E.P.C., C.Y., S.V., L.F.S.), Howard Hughes Medical Institute (J.D.S.), and Department of Pharmacology (J.D.S.), University of Washington, Seattle; and Howard Hughes Medical Institute and Children's Hospital Medical Center for Molecular Cardiovascular Biology (J.D.M.), Cincinnati, Ohio.

Correspondence to Luis F. Santana, PhD, 1705 NE Pacific St HSB-G424, Box 357290, Seattle, WA 98195. E-mail santana@uw.edu



*Circulation Research* **is available at http://circres.ahajournals.org** **DOI: 10.1161/CIRCRESAHA.109.213363**

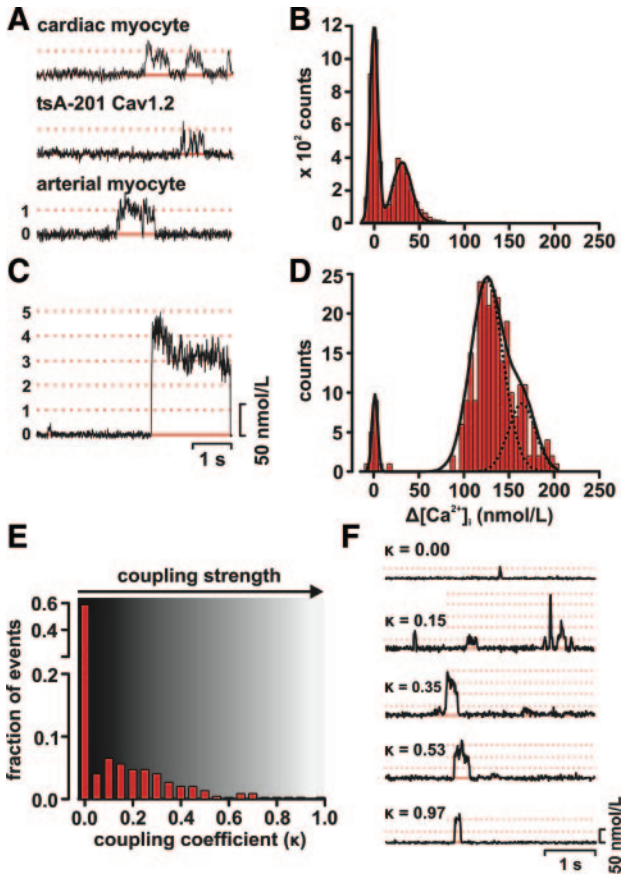


**Figure 1.** Optical recordings of coupled gating of Cav1.2 channels. A, Representative records of $Ca^{2+}$ influx via Cav1.2 channels in neonatal cardiac myocytes (top), tsA-201 cells (middle), and arterial myocytes (bottom). B, All-points histogram of $Ca^{2+}$ sparklet traces in A. The solid black line is the fit ($\chi^2$=2.1) to the data with a multicomponent Gaussian function with centers at 0 and 38 nmol/L. C, $\Delta[Ca^{2+}]_i$ from a $Ca^{2+}$ sparklet site in an arterial myocyte with coupled Cav1.2 channels. D, All-points histogram of the $Ca^{2+}$ sparklet trace in C. The solid black line is the best-fit ($\chi^2$=2.5) to the data with a 3-component Gaussian function with centers at 0, 120, and 160 nmol/L. E, Histogram of the coupling coefficients ($\kappa$) of multiple $Ca^{2+}$ sparklet records from cardiac, arterial, and tsA-201 cells. F, $Ca^{2+}$ sparklet records with varied $\kappa$ values.

(Department of Molecular Physiology and Biophysics, Vanderbilt University, Nashville, Tenn) (PKC$\alpha$).

## Coupled Markov Chain Model

We implemented a coupled Markov chain model in Matlab to determine the coupling coefficient ($\kappa$) among Cav1.2 channels underlying membrane currents and $Ca^{2+}$ sparklet sites. The model was originally developed by Chung and Kennedy[14] to analyze individual records of partially coupled GABA-activated chloride channels.

## Electrophysiology, Confocal, and Total Internal Reflection Fluorescence Microscopy

Voltage-clamp experiments were performed using standard patch-clamp techniques. Total internal reflection fluorescence (TIRF) images were acquired using a through-the-lens TIRF microscope. Images were acquired at 100 to 200 Hz. $Ca^{2+}$ sparklets were detected and defined for analysis using an automated algorithm.[5] Some experiments involved a Nikon swept field confocal system.

## Statistics

Data are presented as means±SEM. A probability value of less than 0.05 was considered significant. The asterisk (*) symbol is used in the figure to illustrate a significant difference between groups.

**Non-standard Abbreviations and Acronyms**

| | |
|---|---|
| **AKAP150** | A-kinase anchoring protein 150 |
| **CaM** | calmodulin |
| **CaMKII** | $Ca^{2+}$/calmodulin-dependent kinase II |
| **EGFP** | enhanced green fluorescent protein |
| **FRET** | fluorescence resonance energy transfer |
| **PDBu** | phorbol 12,13-dibutyrate |
| **PKC** | protein kinase C |
| **RyR** | ryanodine receptor |
| **TIRF** | total internal reflection fluorescence |
| **TS** | Timothy syndrome |
| **tRFP** | tag red fluorescent protein |
| **WT** | wild type |

# Results

## Optical Recordings of Coupled L-Type $Ca^{2+}$ Channels

A TIRF microscope was used to image $Ca^{2+}$ sparklets in arterial smooth muscle cells, neonatal ventricular myocytes, and tsA-201 cells expressing WT Cav1.2 channels. All $Ca^{2+}$ sparklet experiments were performed in voltage clamped cells using the whole-cell configuration of the patch-clamp technique. $Ca^{2+}$ sparklets were recorded in cells treated with the SERCA pump inhibitor thapsigargin (1 $\mu$mol/L) to eliminate $Ca^{2+}$ release from intracellular $Ca^{2+}$ stores. To image $Ca^{2+}$ sparklets, cells were dialyzed with a patch pipette solution containing the fluorescent $Ca^{2+}$ indicator fluo-5F and EGTA. The inclusion of the relatively slow $Ca^{2+}$ buffer EGTA (on rate ≈100-fold slower than fluo-5F) in the intracellular solution serves an important purpose: it restricts fluo-5F fluorescence to the site of $Ca^{2+}$ entry (≈1 $\mu$m). This occurs because with EGTA in the cytosol, $Ca^{2+}$ entering the cell initially interacts with the faster fluo-5F, producing a fluorescence signal, but then quickly (≈2 ms) binds to the more abundant and nonfluorescent EGTA. Thus, in our TIRF experiments, $[Ca^{2+}]_i$ signals are limited to the submembrane space near the mouth of surface membrane $Ca^{2+}$ channels.

Figure 1A shows representative $Ca^{2+}$ sparklets from arterial smooth muscle cells, neonatal ventricular myocytes, and tsA-201 cells expressing Cav1.2 channels. These $Ca^{2+}$ sparklets were recorded while cells were held at −70 mV to increase the driving force for $Ca^{2+}$ influx and maintain a low L-Type $Ca^{2+}$ channel activity, which increased contrast and hence our ability to detect discrete $Ca^{2+}$ entry sites. A $\Delta[Ca^{2+}]_i$ amplitude histogram of these records revealed 2 discrete peaks corresponding to closed channels ($\Delta[Ca^{2+}]_i$=0 nmol/L) and openings of ≈38 nmol/L, which as demonstrated previously, represents the amplitude of quantal $Ca^{2+}$ sparklet events in tsA-201 cells expressing Cav1.2 and arterial myocytes.[5,6,15] A previous study[6] suggested that quantal $Ca^{2+}$ sparklets are likely produced by the opening of a single $Ca^{2+}$ channel.

It is important to note that, consistent with previous work,[5,6] $Ca^{2+}$ sparklet activity in smooth muscle cells, neonatal ventricular myocytes, and tsA-201 cells transfected with Cav1.2 was rapidly eliminated by the application of the

L-Type $Ca^{2+}$ channel inhibitor nifedipine (10 μmol/L) or by superfusion of a $Ca^{2+}$-free external solution (data not shown). Importantly, and as reported recently,[5] $Ca^{2+}$ sparklets were never observed in untransfected tsA-201 cells. Furthermore, $Ca^{2+}$ sparklets in arterial and neonatal ventricular myocytes have the same amplitude of quantal event, activity, and pharmacology (eg, insensitive to 1 μmol/L thapsigargin, eliminated by 10 μmol/L nifedipine) as $Ca^{2+}$ sparklets in tsA-201 cells expressing Cav1.2 channels.[5,15] Collectively these observations strongly suggest that $Ca^{2+}$ sparklets in arterial smooth muscle cells, neonatal ventricular myocytes, and tsA-201 cells expressing Cav1.2 channels are produced by $Ca^{2+}$ influx via L-Type $Ca^{2+}$ channels.

Although most $Ca^{2+}$ sparklets recorded in these cells were similar to those in Figure 1A, we noticed that in a number of $Ca^{2+}$ sparklet sites (191 of 491 sites) small clusters of Cav1.2 channels opened and closed simultaneously to promote greater elevation in subcellular $[Ca^{2+}]_i$ (Figure 1C). The $\Delta[Ca^{2+}]_i$ histogram of the trace in Figure 1D had 3 distinct peaks at a $\Delta[Ca^{2+}]_i$ of 0, 120, and 160 nmol/L. The peaks at 120 and 160 nmol/L likely resulted from the simultaneous activation of 3 and 4 Cav1.2 channels, respectively. Note the absence of a peak near the quantal amplitude of $Ca^{2+}$ influx (ie, 38 nmol/L) in this record. Examples of records with sequential quantal and multi-channel openings are shown in Figures 4A and 5A below.

The observation of $Ca^{2+}$ sparklets resulting from the simultaneous openings of small clusters of Cav1.2 channels is surprising because the $P_o$ of a single Cav1.2 channel is only $\approx 10^{-6}$ at −70 mV.[16] The probability of independently gating channels opening simultaneously at this potential should be very low: $\approx 10^{-12}$, $10^{-18}$, and $10^{-24}$ for the random, coincident opening of 2, 3, or 4 channels. Thus, the probability of observing simultaneous openings of $Ca^{2+}$ channels should be progressively lower as the number of participating channels increase, which should result in a histogram with peaks of decreasing amplitudes as multichannel events become rarer. On the basis of that analysis, $Ca^{2+}$ sparklet events like the one in Figure 1C should be very rare. Yet, $Ca^{2+}$ sparklets resulting from the coincident activation of 2 or more Cav1.2 channels were frequently observed. This suggests that this is not simply the consequence of overlapping stochastic openings of independently activated Cav1.2 channels. Rather, our data provide evidence for the coordinated activation of a small cluster of these channels.

To test this hypothesis, we implemented a coupled Markov chain model to determine the coupling coefficient ($\kappa$) among Cav1.2 channels within $Ca^{2+}$ sparklet sites (Figure 1E and 1F). The model was originally developed by Chung and Kennedy[14] and used to analyze individual records of partially coupled GABA-activated chloride channels. Briefly, this model is a simplified Markov chain model with only 3 free parameters that takes the form of a set of binary chains that are interdependent according to a lumped coupling coefficient parameter called $\kappa$. The other 2 parameters (called $\rho$ and $\varsigma$) describe the intrinsic characteristics of the binary chains. The $\kappa$ value could range from 0 for independently gating channels to 1 for "tightly" coupled channels that open and close simultaneously all the time. A detailed description of this model is provided in the expanded Methods section (Online Data Supplement).

Using this analysis, we found that although the majority of $Ca^{2+}$ sparklets (59%) were likely the result of $Ca^{2+}$ influx via independently gating Cav1.2 channels (ie, $\kappa=0$), numerous $Ca^{2+}$ sparklets were produced by Cav1.2 channels with a $\kappa > 0$. Indeed, the coupling coefficient of nonindependent events (ie, $\kappa > 0$) ranged from 0.1 to 1 with a median value of 0.2. Together with the $Ca^{2+}$ sparklet data above, this Markov analysis suggested that a subpopulation of Cav1.2 channels was capable of gating coordinately.

## Electrophysiological Recordings of Coupled L-Type $Ca^{2+}$ Channels

We used electrophysiological techniques to record L-Type $Ca^{2+}$ channel currents (Figure 2). In these experiments, we recorded elementary L-Type $Ca^{2+}$ channel currents from cell-attached patches from neonatal ventricular myocytes. L-Type $Ca^{2+}$ channel currents were evoked by a 2 s step depolarization to −30 mV from the holding potential of −80 mV. The patch pipette solution contained 20 mmol/L $Ca^{2+}$ (charge carrier), 10 μmol/L tetrodotoxin, 130 mmol/L $TEA^+$ and no $Na^+$ or $K^+$ to eliminate $Na^+$ and $K^+$ channel currents. The L-Type $Ca^{2+}$ channel opener BayK-8644 (500 nmol/L) was included in the pipette solution to increase the mean open time and $P_o$ of these channels and the probability of PKC$\alpha$-dependent, persistent L-Type $Ca^{2+}$ channel activity.[5]

As expected from our $Ca^{2+}$ sparklet studies, depolarization to −30 mV evoked relatively low levels of $Ca^{2+}$ channel activity in most (112 of 134 sweeps, or 84%; from 5 cells) of the sweeps examined (Figure 2A). A current amplitude histogram from these records show 2 distinct peaks with centers at 0 pA (ie, closed channel) and 0.53 pA, which corresponds to the expected single channel current level for an L-Type $Ca^{2+}$ channel at −30 mV with 20 mmol/L $Ca^{2+}$[16]. The $\kappa$ value of the Cav1.2 channels in these patches was 0, suggesting that these currents were produced by independently gating channels. At this point it is important to note that in control experiments inclusion of 10 μmol/L nifedipine prevented all $Ca^{2+}$ channel activity, indicating that L-Type $Ca^{2+}$ channels produced these currents (inset in Figure 2B).

Consistent with our $Ca^{2+}$ sparklet data, we found that in a minority of the records (22 out 134 sweeps or 16%; from 5 cells) membrane depolarization to −30 mV evoked elementary as well as relatively large currents that were likely produced by the simultaneous opening and closing of multiple L-Type $Ca^{2+}$ channels (Figure 2C). The amplitude histogram of the current records in Figure 2C had 4 prominent peaks at 0.0, 0.5, 1.0, and 2.9 pA, likely resulting from the activation of a single or simultaneous activation of 2 or 6 L-Type $Ca^{2+}$ channels, respectively. Closer examination (Figure 2E) of one of the large current events highlighted by the gray box in the bottom sweep in Figure 2C, indicates that in this patch 5 to 6 channel likely opened and then closed simultaneously multiple times. Three additional multichannel current events of similar amplitude were observed in this sweep. As noted above, the prominence of the peak with a center at 3.1 pA in the histogram in Figure 2E and absence of peaks of larger amplitude between this peak and the peak at

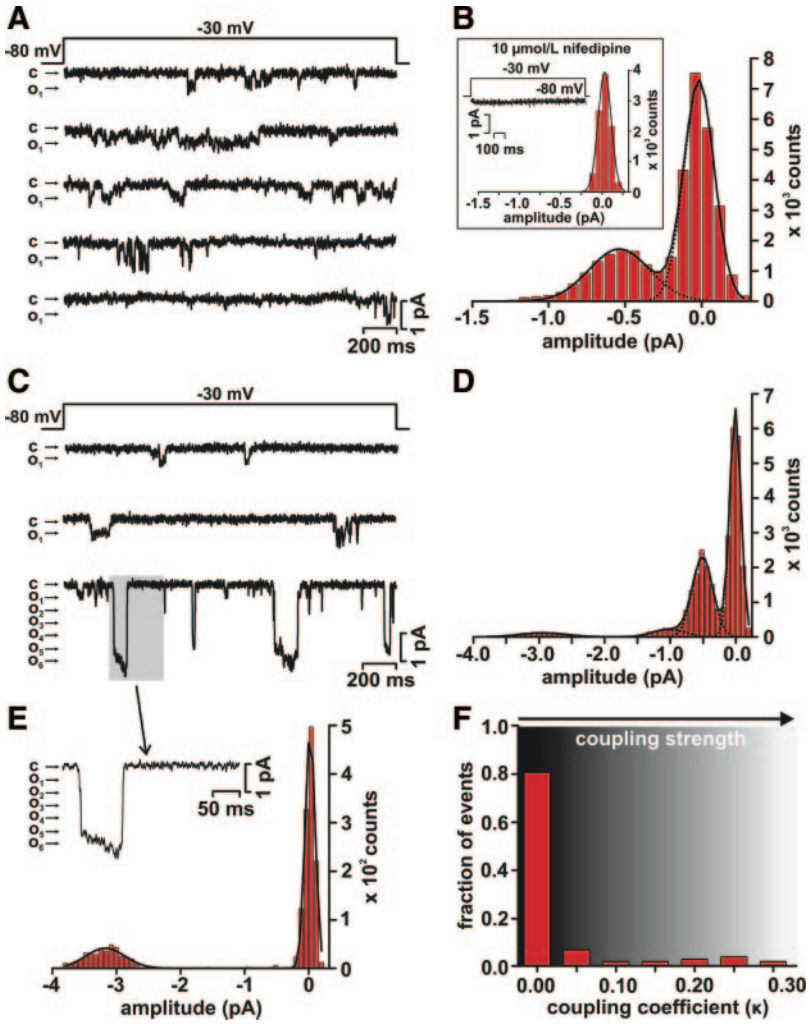


**Figure 2.** Electric recordings of coupled L-Type $Ca^{2+}$ channels. A, Representative elementary L-Type $Ca^{2+}$ channel records obtained during a step depolarization (2 seconds) from −80 to −30 mV. Openings are shown as downward deflections, with the close state denoted by "c," and the open state by "o." B, Histogram of L-Type $Ca^{2+}$ currents traces in A. The solid black line is the fit to the data with a multicomponent Gaussian function with centers at 0.0 and 0.5 pA. The inset shows a histogram from a representative record obtained in the presence of 10 μmol/L nifedipine. C, Representative single and coupled L-Type $Ca^{2+}$ channel current records obtained during step depolarizations from −80 to −30 mV. D, Histogram of the L-Type $Ca^{2+}$ currents records in C. The solid black line is the fit to the data with a multicomponent Gaussian function with centers at 0.0, −0.5, −1.0, and −2.9 pA. E, Trace shows a portion (gray box) of the record in C showing a L-Type $Ca^{2+}$ current resulting from the simultaneous opening and closing of multiple channels. A histogram from this portion of the trace is shown below. The histogram was fitted with a Gaussian function with centers at 0.0 and −3.1 pA. F, Histogram of the coupling coefficients (κ) of multiple L-Type $Ca^{2+}$ current records from cell-attached patches from neonatal ventricular myocytes.

0 pA suggests coupled gating between L-Type $Ca^{2+}$ channels. Consistent with this, the coupling coefficient of the L-Type $Ca^{2+}$ channels in this section was 0.22, suggesting this current was produced by partially coupled channels. Indeed, analysis of all L-Type $Ca^{2+}$ channel records indicates that the majority of the currents were likely the result of independent openings of L-Type $Ca^{2+}$ channels (ie, $\kappa=0$; Figure 2F). In combination with the $Ca^{2+}$ sparklet data above, these findings strongly support the hypothesis that small clusters of Cav1.2 channels can open and close coordinately.

## Activation of PKC$\alpha$ Increases Coupled Gating of Cav1.2 Channels

Activation of PKC$\alpha$ has been linked to elevated persistent $Ca^{2+}$ sparklet activity in arterial myocytes.[5,6,9] Thus, we investigated whether membrane translocation and activation of this kinase increases coupled gating of Cav1.2 channels. To do this, we used 2 complementary approaches. First, we generated a chemically-induced PKC$\alpha$ translocation system.[12,13] Briefly, we created an adenoviral vector expressing a FKBP12-rapamycin-binding element (FRB) that is anchored to the plasma membrane via the myristoylation and palmitoylation modification sequence $Lyn_{11}$. This adenoviral vector also expressed PKC$\alpha$ fused to the enhanced green fluorescent protein (EGFP) and a FK506 binding protein. Application of rapamycin promoted heterodimerization of protein domains from FKBP-PKC$\alpha$-EGFP and the membrane anchored FRB. This recruited FKBP-PKC$\alpha$-EGFP to the membrane from the cytosol on addition of rapamycin (Figure 3A). We used this inducible PKC$\alpha$ in neonatal ventricular myocytes and tsA-201 cells expressing Cav1.2. We found that induction of membrane translocation of PKC$\alpha$ (Figure 3A) increased $Ca^{2+}$ sparklet activity and coupled gating of Cav1.2 channels in cardiac myocytes (n=5 cells; Figure 3B) and tsA-201 cells (n=6 cells; Online Figure I).

Our second approach involved the activation of endogenous PKC using the phorbol 12,13-dibutyrate (PDBu) (500 nmol/L). Activation of PKC with PDBu had a similar effect in arterial myocytes (n=17 cells; Figure 3C and 3D). Taken together, these data suggest that membrane translocation and activation of PKC$\alpha$ increases the probability of coupled gating between Cav1.2 channels.

## Movement of Calmodulin Away From the IQ Domain in the C-Tail of Cav1.2 Channels Increases Coupled Gating of These Channels

We observed that the activity of $Ca^{2+}$ sparklets produced by coupled Cav1.2 channels was higher than those produced by independently gating channels (Figure 3E). This raised the intriguing possibility that the probability of coupled gating of

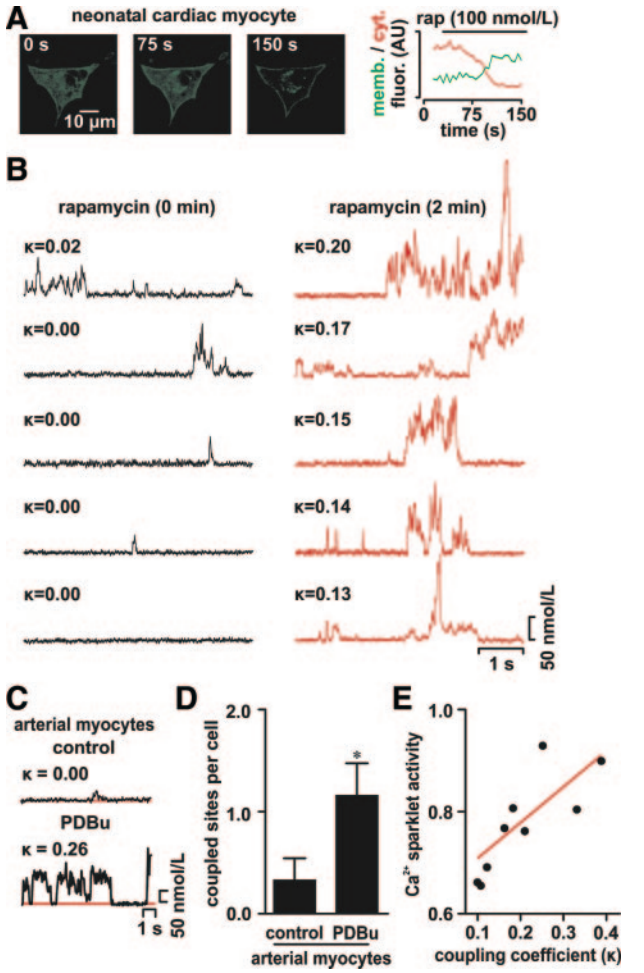


**Figure 3.** Activation of PKC$\alpha$ increases coupled gating between Cav1.2 channels. A, Confocal images of neonatal ventricular cells expressing the inducible PKC$\alpha$ translocation system before (0 second) and after (75 and 150 seconds) application of 0.1 $\mu$mol/L rapamycin to induce membrane translocation of this kinase. The graph on the right shows the time course of PKC$\alpha$ fluorescence intensity in the membrane and cytosol in this cardiac myocyte. $\Delta[Ca^{2+}]_i$ records from multiple $Ca^{2+}$ sparklet sites before (left) and after (right) induction of PKC$\alpha$-EGFP translocation are shown below the confocal images (B). The $\kappa$ of the Cav1.2 channels in this site is shown above each record. C, $Ca^{2+}$ sparklet records from an arterial myocyte before and after PDBu (500 nmol/L). D, Bar plot of the mean number of coupled sites per cell in arterial myocytes under control condition and after application of 500 nmol/L PDBu. E, Relationship between $Ca^{2+}$ sparklet activity and coupling coefficient. Red line is a linear fit to the data ($r^2$=0.64).

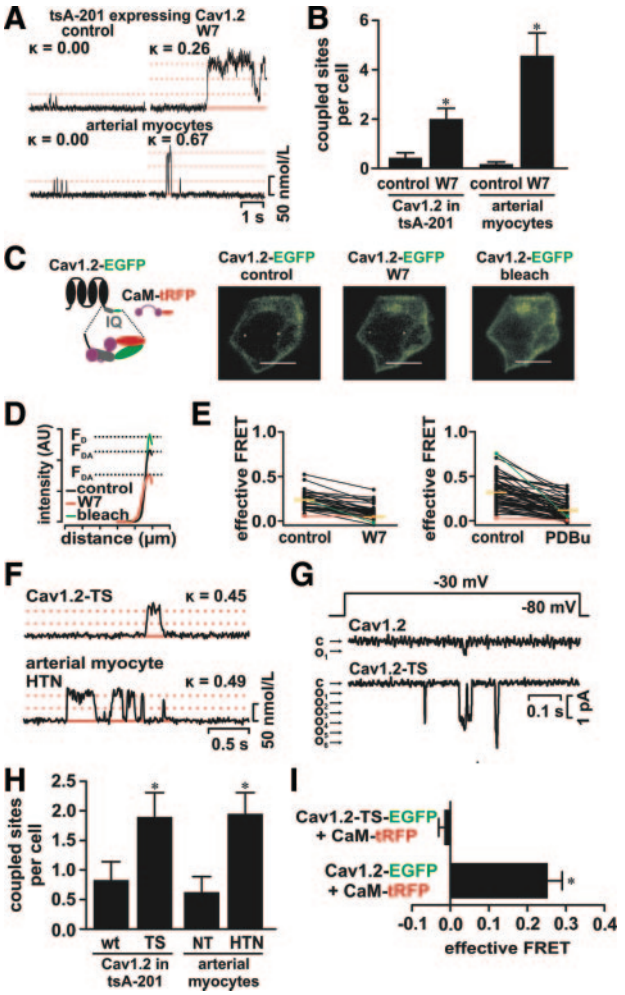


**Figure 4.** Displacing CaM from the IQ domain of Cav1.2 increases coupled gating of WT and TS Cav1.2 channels. A, $Ca^{2+}$ sparklet records from tsA-201 and arterial myocytes showing induction of coupled gating by W7 (100 $\mu$mol/L). Kappa values are shown above each trace. B, Number of coupled sites per cell before and after W7. C, Illustration of Cav1.2-EGFP and CaM-tRFP. Right, Images of Cav1.2-EGFP in tsA-201 cells under control conditions, during W7 treatment, and following CaM-tRFP photobleaching. D, Cav1.2-EGFP fluorescence intensity at an example cross-section of the membrane marked by the white line in each of the images in C. Dotted lines show the $F_{DA}$ and $F_A$ values used to calculate effective FRET=1−($F_{DA}$/$F_A$). E, FRET in specific sites before and after W7 (center, lower row) or PDBu (right, lower row) application. Yellow bars are mean values. F, $Ca^{2+}$ sparklet records with coupled Cav1.2 channels from tsA-201 cells expressing Cav1.2-TS and hypertensive smooth muscle. G, Representative Cav1.2 channel currents evoked by depolarization from −80 to −30 mV in patches (cell-attached) from tsA-201 cells expressing WT (upper trace) and Cav1.2-TS channels (lower trace). The close state is denoted by a "c" and the open state by an "o." H, Number of sites with coupled Cav1.2 channels per cell in cells expressing WT and TS Cav1.2 and in normotensive (NT) and hypertensive (HTN) smooth muscle. I, FRET data between EGFP-tagged WT or TS Cav1.2 and CaM-tRFP.

Cav1.2 channels might be enhanced by deficient $Ca^{2+}$-dependent inactivation (CDI) of these channels. CaM mediates CDI of Cav1.2 channels.[17,18] Thus, we tested the hypothesis that inhibition of CaM increases the probability of coupled gating of Cav1.2 channels.

Consistent with this hypothesis, we found that application of the CaM antagonist W7 (100 $\mu$mol/L) increased the number of sites with coupled Cav1.2 channels ≈7-fold and 27-fold in tsA-201 cells (n=4 cells) and myocytes (n=7 cells), respectively ($P$<0.05; Figure 4A and 4B). Similar findings were obtained in myocytes injected with the CaM-inhibitory peptide (1 $\mu$mol/L; n=4 cells; expanded Methods section [Online Data Supplement] and Online Figure II). Application of either CaM antagonist increased the number of $Ca^{2+}$ sparklet sites with coupled Cav1.2 channels, but not the median $\kappa$ value (0.2) of coupled channels ($P$>0.05).

To examine the dynamics of this phenomenon, we used FRET to visualize the interaction between Cav1.2 channels

and CaM. The C terminus of Cav1.2 was tagged with the EGFP (Cav1.2-EGFP) and CaM was fused with tag red fluorescent protein (CaM-tRFP) (Figure 4C and 4D). CaM associates with the IQ domain in the C terminus of Cav1.2, which is critical for CDI of these channels.[17,19] Accordingly, FRET was relatively high (0.32±0.02, n=10 cells) between Cav1.2-EGFP and CaM-tRFP under control conditions. Application of the CaM antagonist W7 (100 μmol/L) or the PKC activator PDBu (500 nmol/L) decreased FRET between Cav1.2-EGFP and CaM-tRFP from 0.21±0.04 to 0.08±0.03 (n=10 cells) and from 0.33±0.02 to 0.12±0.10 (n=11 cells), respectively (Figure 4E) ($P<0.05$). Note, however, that the magnitude of the decrease in FRET induced by W7 and PKCα activation varied within cells. The relative change in FRET ranged from 0 in some sites (red line in Figure 4E) to 100% in others (green line in Figure 4E). A decrease in FRET suggests an increase in the distance between Cav1.2-EGFP and CaM-tRFP. This could result from 2 potential scenarios. *First*, CaM-tRFP dissociates from the IQ domain of Cav1.2-EGFP channels. *Second*, CaM-tRFP changes in position within the C tail of Cav1.2 channels, moving away from the EGFP fused to the C terminus of these channel enough to decrease or even eliminate FRET. Although our FRET experiments cannot distinguish between these 2 possibilities, they evidently suggest that displacement of CaM away from the IQ domain of Cav1.2 channels may be a critical step in the induction of coupled gating of these channels.

## Increased Coupled Gating of Cav1.2 Channels During Hypertension and TS

Increased Cav1.2 channel activity underlies lethal cardiac arrhythmias and autism in humans with TS.[20] In TS, a single amino acid substitution (Gly-436-Arg) in Cav1.2 (Cav1.2-TS) increases the open time and $P_o$ of these channels.[11,20] We recorded $Ca^{2+}$ sparklets (−70 mV) and depolarization-evoked currents in tsA-201 cells expressing WT and Cav1.2-TS channels (Figure 4F and 4G, respectively). We found a higher frequency of $Ca^{2+}$ sparklets with coupled Cav1.2 channels in tsA-201 cells expressing Cav1.2-TS (n=10 cells) than WT channels (n=10 cells; Figure 4H; $P<0.05$).

Next, we used experimental conditions similar to those used to record $Ca^{2+}$ currents in neonatal cardiac myocytes above. Membrane depolarization to −30 mV activated WT and Cav1.2-TS channels in tsA-201 cells. Voltage-activated $Ca^{2+}$ currents were never recorded in untransfected tsA-201 cells. As in neonatal myocytes, the amplitude of the elementary $Ca^{2+}$ currents activated by a voltage pulse to −30 mV was similar (0.49±0.01 pA) to that in neonatal ventricular myocytes (0.53±0.01 pA; $P>0.05$). This observation gives further support to the view that Cav1.2 channels produced the currents recorded in neonatal myocytes. Consistent with our $Ca^{2+}$ sparklet studies, we recorded a number of $Ca^{2+}$ currents resulting from the simultaneous opening and closing (ie, coupled gating) of channels in cells expressing Cav1.2-TS than WT Cav1.2 (Figure 4G).

Increased L-Type $Ca^{2+}$ channel activity in arterial myocytes has been implicated in the chain of events that leads to vascular dysfunction during hypertension.[21,22] In hypertensive arterial myocytes, higher Cav1.2 channel activity is due, at least in part, to increased local PKCα activity. We found a higher frequency of coupled Cav1.2 channel gating events both in arterial myocytes from an animal model of angiotensin II–induced hypertension and in tsA-201 cells expressing Cav1.2-TS channels (Figure 4F and 4H).

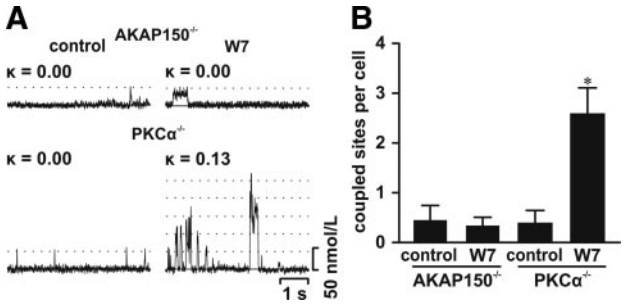


**Figure 5.** AKAP150, but not PKCα, is required for coupled gating of Cav1.2 channels. A, Representative $\Delta[Ca^{2+}]_i$ records from $Ca^{2+}$ sparklet sites in AKAP150$^{-/-}$ and PKCα$^{-/-}$ smooth muscle cells under control conditions (right) and after exposure to 100 μmol/L W7. The coupling coefficient (κ) of these Cav1.2 channels is shown above each trace. Dotted lines show the amplitude of quantal levels. B, Bar plot of the mean number of coupled sites per cell.

We investigated whether, as with WT Cav1.2 channels, the higher frequency of coupled gating events of Cav1.2-TS channels was associated with displacement of CaM from the IQ domain in the C terminal of these channels. Accordingly, FRET between Cav1.2-TS-EGFP and CaM-tRFP was undetectable (n=13 cells; Figure 4I). These data suggest that coupled gating of Cav1.2 channels is associated with displacement of CaM away from the IQ domain in the C-terminal tail and contributes to enhanced channel function and $Ca^{2+}$ influx during hypertension and TS.

## AKAP150 Increases the Probability of Coupled Gating Between Cav1.2 Channels

The scaffolding protein AKAP150 targets PKCα to the cell membrane[23] and interacts with the C tail of Cav1.2 channels.[24] Therefore, we tested the hypothesis that PKCα activation and its targeting to the membrane by AKAP150 is necessary to induce coupled gating of Cav1.2 channels during CaM inhibition (Figure 5). Application of W7 increased the number of coupled Cav1.2 channel events in PKCα null (PKCα$^{-/-}$; n=5 cells), but not in AKAP150 null myocytes (AKAP150$^{-/-}$; n=9 cells; $P<0.05$). Because the expression of PKCα is similar in WT and AKAP150$^{-/-}$ myocytes,[9] the lack of effect of W7 on Cav1.2 channels in AKAP150$^{-/-}$ was not attributable to decreased PKCα expression. These data suggest that CaM antagonists work downstream of PKCα and that AKAP150 participates in the molecular events that facilitate coupled gating of Cav1.2 channels.

## Coupling of Cav1.2 Channels Involves Interactions Between Neighboring Channels via Their C Termini

We investigated the role of the C terminus of Cav1.2 channels in coupled gating. To do this, a Cav1.2 construct lacking amino acids 1670 to 2171 (Cav1.2Δ1670X), which eliminates a large section of the C-terminal tail, was expressed in tsA-201 cells (Figure 6A). These channels lack the putative AKAP-binding

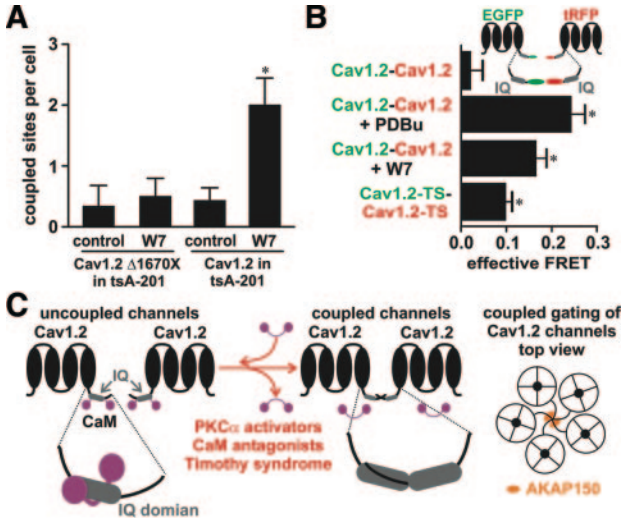


**Figure 6.** Coupled gating involves the C tail of Cav1.2 channels. A, Bar plot of number of sites showing coupling of Cav1.2 channels in cells expressing a truncated Cav1.2 channel (Cav1.2Δ1670X) or WT Cav1.2 channels before and after application of 100 μmol/L W7. B, Bar plot of effective FRET between Cav1.2-TS-EGFP and Cav1.2-TS-tRFP or WT Cav1.2-EGFP and Cav1.2-tRFP before and after PDBu or W7. The inset shows an illustration of Cav1.2-EGFP and Cav1.2-tRFP. C, Proposed model for coupled gating of Cav1.2 channels.

region.[24] Unlike WT channels, Cav1.2Δ1670X channels showed no coupled gating activity under either control conditions or after the application of W7 (n=5 cells), indicating that residues 1670 to 2171 of Cav1.2 are critical for coupled gating activity.

The C termini of Cav1.2 channels could be involved in coupled gating by coming into close proximity. To examine this possibility, we expressed WT and TS Cav1.2 channels with EGFP or tRFP fused to their C termini and determined FRET between channels (Figure 6B). Under control conditions, FRET between WT Cav1.2-EGFP and Cav1.2-tRFP was low (0.02±0.02; n=10 cells). This is consistent with the observation of a relatively low frequency of coupled Cav1.2 events under these experimental conditions (see Figure 1 above). Application of W7 or PDBu, which increases coupled gating of Cav1.2 channels, increased FRET between WT Cav1.2-EGFP and Cav1.2-tRFP channels to 0.16±0.02 (n=8 cells) and 0.23±0.03 (n=10 cells), respectively ($P<0.05$). Interestingly, under control conditions, FRET was higher in cells expressing tRFP- and EGFP-tagged Cav1.2-TS channels (0.10±0.01; n=10 cells) than between WT Cav1.2 channels ($P<0.05$; Figure 6B). These data suggest that the C termini of Cav1.2 channels come into close proximity under conditions that favor coupled gating.

## Discussion

In this study, we demonstrated that a cluster of Cav1.2 channel proteins can be organized to facilitate their coordinated opening and closing. A cartoon of the proposed model for coupled gating of Cav1.2 channels is shown in Figure 6C. Our data suggest that CaM antagonists (eg, W7 and CaM inhibitory peptide), activators of PKCα, or a specific Cav1.2 channel mutation (eg, TS), that move CaM away from the IQ domain in the C-terminal tail of the channel promote coupled gating between Cav1.2 channels. Although at present the exact mechanisms underlying coupled gating between Cav1.2 are unclear, our FRET analysis of EGFP- and tRFP-tagged Cav1.2 channels suggests the possibility that coupled gating between these channels may involve transient interactions between a variable number (2-6 channels) of adjacent channels via their C termini. A recent report suggesting that the C terminus of Cav1.2 channels dimerizes in vitro[25] gives additional credence to this view.

An important feature of our model is that AKAP150 increases the probability of coupled gating presumably by facilitating interactions between the C termini of Cav1.2. Because AKAP150 interacts with only a subpopulation of Cav1.2 channels,[9] this scaffolding protein promotes coupled gating in a fraction of channels, resulting in subcellular variations in Cav1.2 activity. This represents a novel function of AKAP150 that is independent of its ability to target proteins to specific regions of the cell.

In our model, the level of expression of AKAP150 is a critical determinant of coupled Cav1.2 channel activity in cardiac and smooth muscle cells for multiple reasons. We demonstrated that PKCα increases the frequency of coupled gating events. Interestingly, in the TS, the Gly-436-Arg substitution in Cav1.2 creates a putative phosphorylation site for $Ca^{2+}$/CaM-dependent kinase (CaMK)II.[11] The actions of PKCα and CaMKII on WT and Cav1.2-TS are opposed by the $Ca^{2+}$/CaM-dependent phosphatase calcineurin. Note, however, that AKAP150 targets PKCα and calcineurin to the surface membrane. Accordingly, the level of coupled gating events between Cav1.2 channels may not be simply limited by AKAP150 expression, but also by the relative activities of nearby calcineurin, CaMKII, and PKCα.

These conditions for coupled gating between Cav1.2 channels impose technical challenges for the recording and analysis of the molecular mechanisms underlying these events. For example, because only a subpopulation of Cav1.2 channels could undergo coupled gating, the use of patch-clamp approaches to record currents from relatively small areas of the membrane is likely to yield limited results in terms of the number of couple gating events per trial. However, our study suggests that optical recordings of Cav1.2 channels from relatively large portions of the surface may represent a more efficient approach to study coupled gating between these channels. For the same reasons, conventional biochemical approaches (eg, coimmunoprecipitation) broadly used to examine direct, stable protein-protein interactions could be difficult to implement to study the molecular mechanisms of coupled gating between Cav1.2 channels. FRET could be used to circumvent these limitations. However, although powerful, this technique has its limitations because it reports the proximity of 2 fluorescent proteins (in our case EGFP and tRFP) and not necessarily the specific sections of the channel to which they are fused. Thus, currently, whether coupled gating between Cav1.2 channels involves direct physical interactions between the C tails of adjacent channels or to an intermediary protein such as AKAP150 and how this translates into the simultaneous opening and closing of their pores is unclear. Future experiments should address this critical issue.

Our data provide insights into the mechanisms by which PKCα could induce coupled gating between Cav1.2 channels. We found that PKC activation moves CaM away from the IQ domain of Cav1.2 channels. Yet, although PKCα increases coupled Cav1.2 channel activity, this kinase was not required

for the induction of coupled activity because application of W7 induced coupled gating of Cav1.2 channels in PKC$\alpha^{-/-}$ arterial myocytes. Together, these findings suggest that PKC$\alpha$ activation promotes coupled gating between Cav1.2 channels by inducing the movement of CaM away from the IQ domain in the C tail of Cav1.2. However, our data indicate that phosphorylation of Cav1.2 channel by this kinase per se is not necessary to induce coupled gating. Subsequent studies should examine if a similar mechanism is involved in coupled gating between Cav1.2-TS channels.

An intriguing observation in this study is that coupling between Cav1.2 channels is transient, with the number of channels opening and closing simultaneously varying with time and between sites. In many instances, we saw sets of 2, 3, 4, 5 and 6 channels opening and closing together. We did not detect a particular pattern in terms of the number of channels undergoing coupled gating. This coupling mechanism is fundamentally different from that of ryanodine receptors (RyRs) in cardiac muscle,[26] in which tetramers of tightly coupled (ie, $\kappa \approx 1$) channels undergo stable openings under physiological conditions. At present, the precise mechanisms that control the coupling strength between Cav1.2 channels and how it changes under physiological (eg, changes in membrane potential) and pathological conditions is unclear.

Although the effects of coupled gating of Cav1.2 channels on excitation-contraction (EC) coupling in cardiac and smooth muscle were not examined in this study, previous studies suggest coupling of these channels could have important implications in this process. In ventricular myocytes, Cav1.2 channels and RyRs in nearby junctional sarcoplasmic reticulum form a functional unit called a "couplon."[27] $Ca^{2+}$ influx via Cav1.2 activates small clusters of RyRs via the mechanism of $Ca^{2+}$-induced $Ca^{2+}$ release, producing $Ca^{2+}$ sparks. In these cells, activation of multiple couplons during an action potential results in a cell-wide increase in $[Ca^{2+}]_i$ that activates contraction. Because the probability of $Ca^{2+}$ spark occurrence ($P_{Spark}$) is proportional to the Cav1.2 current and local $[Ca^{2+}]_i$,[28] it is intriguing to speculate that $P_{Spark}$ is likely to be higher in couplons with coupled Cav1.2 channels than in couplons with independently gating channels. Unlike ventricular myocytes, in smooth muscle, Cav1.2 channels and RyRs are not tightly coupled. In these cells, activation of Cav1.2 channels results in an increase in $[Ca^{2+}]_i$ that directly activates contractile proteins. Thus, an increase in coupled gating of Cav1.2 channels could result in an increase in $Ca^{2+}$ influx and thus global $[Ca^{2+}]_i$. Subsequent studies should test these intriguing hypotheses.

To conclude, we propose that coupled gating of Cav1.2 channels could translate into a larger increase in L-Type $Ca^{2+}$ channel activity than by an increase in independent gating activity. The simultaneous activation of a small cluster of channels would enhance $Ca^{2+}$ influx per gating event. Under physiological conditions, this could increase the activation probability of $Ca^{2+}$-dependent proteins involved in contraction, excitability, memory, and gene expression. In TS, coupled gating of Cav1.2 channels could increase the probability of $Ca^{2+}$-dependent arrhythmias and increase $Ca^{2+}$-dependent neurotoxicity. In hypertensive smooth muscle, coupled gating of Cav1.2 channels could increase myogenic tone and hence blood pressure. We propose that coupled gating of Cav1.2 channels may represent a general mechanism that contributes to $Ca^{2+}$ influx and excitability under physiological and pathological conditions.

## Acknowledgments

We thank Drs Bertil Hille, Carmen A. Ufret-Vincenty, and Madeline Nieves-Cintrón for reading this manuscript.

## Sources of Funding

Supported by grants from NIH (HL085870, HL85686, and HL088366), the Leducq Foundation (cycAMP ObCDV), and the American Heart Association (0735251N and 0840094N).

## Disclosures

None.

## References

1. Gomez-Ospina N, Tsuruta F, Barreto-Chang O, Hu L, Dolmetsch R. The C terminus of the L-Type voltage-gated calcium channel Ca(V)1.2 encodes a transcription factor. *Cell*. 2006;127:591–606.
2. Fourcaudot E, Gambino F, Casassus G, Poulain B, Humeau Y, Luthi A. L-Type voltage-dependent $Ca^{2+}$ channels mediate expression of presynaptic LTP in amygdala. *Nat Neurosci*. 2009;12:1093–1095.
3. Cannell MB, Berlin JR, Lederer WJ. Effect of membrane potential changes on the calcium transient in single rat cardiac muscle cells. *Science*. 1987;238:1419–1423.
4. Marrion NV, Tavalin SJ. Selective activation of $Ca^{2+}$-activated $K^+$ channels by co-localized Ca2+ channels in hippocampal neurons. *Nature*. 1998;395:900–905.
5. Navedo MF, Amberg GC, Nieves M, Molkentin JD, Santana LF. Mechanisms Underlying Heterogeneous $Ca^{2+}$ Sparklet Activity in Arterial Smooth Muscle. *J Gen Physiol*. 2006;127:611–622.
6. Navedo MF, Amberg G, Votaw SV, Santana LF. Constitutively active L-Type $Ca^{2+}$ channels. *Proc Natl Acad Sci U S A*. 2005;102:11112–11117.
7. Tour O, Adams SR, Kerr RA, Meijer RM, Sejnowski TJ, Tsien RW, Tsien RY. Calcium Green FlAsH as a genetically targeted small-molecule calcium indicator. *Nat Chem Biol*. 2007;3:423–431.
8. Wang SQ, Song LS, Lakatta EG, Cheng H. $Ca^{2+}$ signalling between single L-Type $Ca^{2+}$ channels and ryanodine receptors in heart cells. *Nature*. 2001;410:592–596.
9. Navedo MF, Nieves-Cintrón M, Amberg GC, Yuan C, Votaw VS, Lederer WJ, McKnight GS, Santana LF. AKAP150 is required for stuttering persistent $Ca^{2+}$ sparklets and angiotensin II induced hypertension. *Circ Res*. 2008;102:e1–e11.
10. Devic E, Xiang Y, Gould D, Kobilka B. Beta-adrenergic receptor subtype-specific signaling in cardiac myocytes from beta(1) and beta(2) adrenoceptor knockout mice. *Mol Pharmacol*. 2001;60:577–583.
11. Erxleben C, Liao Y, Gentile S, Chin D, Gomez-Alegria C, Mori Y, Birnbaumer L, Armstrong DL. Cyclosporin and Timothy syndrome increase mode 2 gating of CaV1.2 calcium channels through aberrant phosphorylation of S6 helices. *Proc Natl Acad Sci U S A*. 2006;103:3932–3937.
12. Liberles SD, Diver ST, Austin DJ, Schreiber SL. Inducible gene expression and protein translocation using nontoxic ligands identified by a mammalian three-hybrid screen. *Proc Natl Acad Sci U S A*. 1997;94:7825–7830.
13. Suh BC, Inoue T, Meyer T, Hille B. Rapid chemically induced changes of PtdIns(4,5)P2 gate KCNQ ion channels. *Science*. 2006;314:1454–1457.
14. Chung SH, Kennedy RA. Coupled Markov chain model: characterization of membrane channel currents with multiple conductance sublevels as partially coupled elementary pores. *Math Biosci*. 1996;133:111–137.
15. Navedo MF, Amberg GC, Westenbroek RE, Sinnegger-Brauns MJ, Catterall WA, Striessnig J, Santana LF. Cav1.3 channels produce persistent calcium sparklets, but Cav1.2 channels are responsible for sparklets in mouse arterial smooth muscle. *Am J Physiol Heart Circ Physiol*. 2007;293:H1359–H1370.
16. Rubart M, Patlak JB, Nelson MT. $Ca^{2+}$ currents in cerebral artery smooth muscle cells of rat at physiological $Ca^{2+}$ concentrations. *J Gen Physiol*. 1996;107:459–472.

17. Zuhlke RD, Pitt GS, Deisseroth K, Tsien RW, Reuter H. Calmodulin supports both inactivation and facilitation of L-Type calcium channels. *Nature*. 1999;399:159–162.
18. Imredy JP, Yue DT. Mechanism of $Ca^{2+}$-sensitive inactivation of L-Type $Ca^{2+}$ channels. *Neuron*. 1994;12:1301–1318.
19. Erickson MG, Alseikhan BA, Peterson BZ, Yue DT. Preassociation of calmodulin with voltage-gated $Ca^{2+}$ channels revealed by FRET in single living cells. *Neuron*. 2001;31:973–985.
20. Splawski I, Timothy KW, Sharpe LM, Decher N, Kumar P, Bloise R, Napolitano C, Schwartz PJ, Joseph RM, Condouris K, Tager-Flusberg H, Priori SG, Sanguinetti MC, Keating MT. Ca(V)1.2 calcium channel dysfunction causes a multisystem disorder including arrhythmia and autism. *Cell*. 2004;119:19–31.
21. Pesic A, Madden JA, Pesic M, Rusch NJ. High blood pressure upregulates arterial L-Type $Ca^{2+}$ channels. Is membrane depolarization the signal? *Circ Res*. 2004;94:e97–e104.
22. Nieves-Cintron M, Amberg GC, Navedo MF, Molkentin JD, Santana LF. The control of $Ca^{2+}$ influx and NFATc3 signaling in arterial smooth muscle during hypertension. *Proc Natl Acad Sci U S A*. 2008;105:15623–15628.
23. Klauck TM, Faux MC, Labudda K, Langeberg LK, Jaken S, Scott JD. Coordination of three signaling enzymes by AKAP79, a mammalian scaffold protein. *Science*. 1996;271:1589–1592.
24. Oliveria SF, Dell'Acqua ML, Sather WA. AKAP79/150 anchoring of calcineurin controls neuronal L-Type $Ca^{2+}$ channel activity and nuclear signaling. *Neuron*. 2007;55:261–275.
25. Fallon JL, Baker MR, Xiong L, Loy RE, Yang G, Dirksen RT, Hamilton SL, Quiocho FA. Crystal structure of dimeric cardiac L-Type calcium channel regulatory domains bridged by $Ca^{2+}$* calmodulins. *Proc Natl Acad Sci U S A*. 2009;106:5135–5140.
26. Marx SO, Gaburjakova J, Gaburjakova M, Henrikson C, Ondrias K, Marks AR. Coupled gating between cardiac calcium release channels (ryanodine receptors). *Circ Res*. 2001;88:1151–1158.
27. Franzini-Armstrong C, Protasi F, Ramesh V. Shape, size, and distribution of $Ca^{2+}$ release units and couplons in skeletal and cardiac muscles. *Biophys J*. 1999;77:1528–1539.
28. Santana LF, Cheng H, Gomez AM, Cannell MB, Lederer WJ. Relation between the sarcolemmal $Ca^{2+}$ current and $Ca^{2+}$ sparks and local control theories for cardiac excitation-contraction coupling. *Circ Res*. 1996;78:166–171.

## Novelty and Significance

### What Is Known?

- Increased calcium influx via dihydropyridine-sensitive L-Type calcium channels has been identified in the pathogenesis of diseases such as cardiac arrhythmias, autism, and hypertension.
- Blockade of L-Type calcium channels is currently widely used in the treatment of arrhythmias, angina, and hypertension.
- Not all L-Type calcium channels are equal; some sites of channel activity allow more calcium influx than others.

### What New Information Does This Article Contribute?

- Instead of operating independently, clusters of L-Type calcium channels can be formed spontaneously and transiently, to allow these clusters of channels to open concertedly in a "coupled" manner.
- The observed frequency of these "coupled" L-Type calcium channel openings is significantly increased in diseases such as Timothy syndrome (LQT8) and hypertension.
- When calmodulin has reduced affinity for the L-Type calcium channel, L-Type calcium channels couple more frequently in the presence of AKAP150.

Although it has become clear recently that not all L-Type calcium channels are functionally equal and differences in local calcium concentration can play an important role in excitation–contraction coupling and calcium signaling, we wanted to know whether clusters of L-Type calcium channels can open in a "coupled" fashion as to maximize local calcium elevation. Using optical and electrophysiological approaches, we observed that coupled calcium channel openings and clustering do occur and that their frequency is significantly increased with a Timothy syndrome (LQT8) mutation and in arterial myocytes from hypertensive animals. Furthermore, we described a possible model for these coupled openings. When calmodulin has decreased affinity for the C-terminal tail of the L-Type calcium channel, coupled openings and physical clustering of L-Type calcium channels occur more frequently, as long as A-kinase anchoring protein (AKAP) 150 is present. Therefore, our proposed model is that coupling occurs when calmodulin moves away from the C terminus, allowing for the C-terminal tails to physically interact with the aid of AKAP150. This is a completely novel model that for the first time describes how L-Type calcium channels can act together to bring about greater calcium influx than independent channels. Clinically, our model also suggests potential pharmacological targets for the treatment of arrhythmia and hypertension.

**Supplement Material**

## *Results*

### *Inducible PKCα translocation in tsA-201 cells increases coupled Cav1.2 channel activity*

We recorded $Ca^{2+}$ sparklet activity in voltage-clamped tsA-201 cells (-70 mV) expressing Cav1.2 channels as well as membrane-anchored Lyn11-FRB and FKBP-PKCα-EGFP (Online Figure I). Under control conditions, FKBP-PKCα-EGFP fluorescence was distributed broadly throughout the cytosol of tsA-201 cells. Application of rapamycin (0.1 μmol/L) induced a rapid decrease in cytosolic fluorescence and an increase in membrane-associated fluorescence, which was produced by the translocation of FKBP-PKCα-EGFP to the surface membrane of these cells. The translocation of FKBP-PKCα-EGFP to the sarcolemma of these cells was complete 85 ± 5 seconds (n = 6 cells) after the introduction of rapamycin.

As in neonatal ventricular myocytes, membrane-anchored Lyn11-FRB, and FKBP-PKCα-EGFP (see Figure 3 in the printed version of the manuscript), $Ca^{2+}$ sparklet activity in general and coupled activity in specific was low in tsA-201 cells under control conditions (i.e. -70 mV, before application of rapamycin) (Online Figure IB). However, PKCα translocation to the surface membrane of these cells evoked an increase in coupled Cav1.2 activity in previously active and silent $Ca^{2+}$ sparklet sites ($p < 0.05$).

### *Calmodulin-inhibitory peptide increases coupled gating of Cav1.2 channels*

In these experiments, we used a 17-residue peptide based on the calmodulin (CaM)-binding domain of myosin light chain kinase. This peptide inhibits CaM by binding to it with high affinity ($K_d$ = 6 pM). We tested the hypothesis that the CaM inhibitory peptide increases coupled gating of Cav1.2 channels in arterial myocytes. To test this hypothesis, we recorded $Ca^{2+}$ sparklet activity at -70 mV in control myocytes and in cells dialyzed via the patch pipette with an intracellular solution similar to the one used for control cells, but containing 1 μM of the CaM inhibitory peptide (Online Figure II). As with the CaM antagonist W7 (see Figure 4 in the printed version of the manuscript), we found a higher frequency ($p < 0.05$) of coupled gating Cav1.2 events in cells exposed to the CaM inhibitory peptide than in control cells. Together with the W7 data, these findings strongly suggest that CaM inhibition increases the probability of coupled gating between Cav1.2 channels.

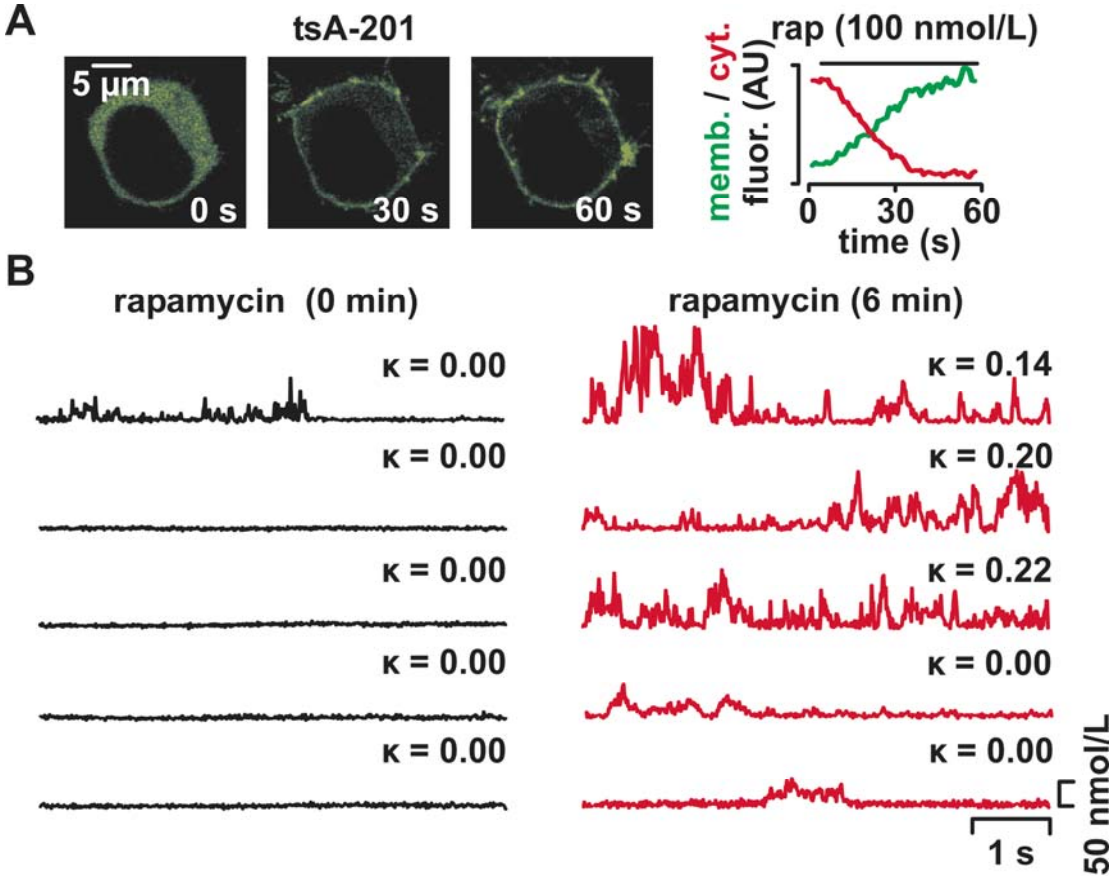


**Online Figure I. Activation of PKCα induces coupled gating of L-type $Ca^{2+}$ channels in tsA-201 cells expressing Cav1.2 channels**. (A) Confocal images of tsA-201 cells expressing FKBP-PKCα-EGFP and membrane-anchored Lyn11-FRB before (0 s) and after (30 and 60 s) application of 0.1 µmol/L rapamycin. The graph on the right side of the images shows the time course of PKCα fluorescence intensity in the membrane (green) and cytosol (red) in this cell. (B) $\Delta[Ca^{2+}]_i$ records from multiple $Ca^{2+}$ sparklet sites (-70 mV) before (left) and after (right) induction of FKBP-PKCα-EGFP translocation. The coupling coefficient (κ) of Cav1.2 at each site is shown above the trace.

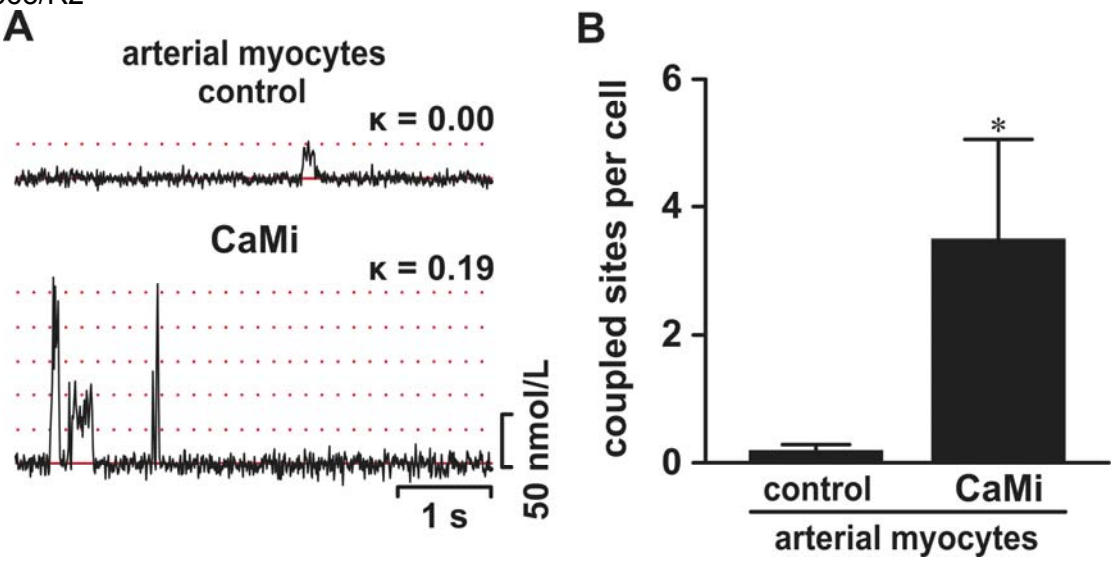


**Online Figure II. CaM-inhibitory peptide increases coupled gating of Cav1.2 channels.** (A) Representative $\Delta[Ca^{2+}]_i$ records from $Ca^{2+}$ sparklet sites in smooth muscle cells under control conditions (top) and during dialysis with the CaM inhibitory (CaMi) peptide (1 μmol/L; bottom). The coupling coefficient (κ) of these Cav1.2 channels is shown above each trace. Dotted lines show the amplitude of quantal levels. (B) Bar plot of the mean number of coupled sites per cell.

## *Methods*

### *Isolation of arterial and adult and neonatal cardiac myocytes*

Mice (PKCα$^{-/-}$, AKAP150$^{-/-}$, and corresponding wild type littermates) and Sprague Dawley (SD) rats were euthanized with a lethal dose of sodium pentobarbital as approved by the University of Washington Institutional Animal Care and Use Committee. Spontaneously beating neonatal cardiac myocytes were prepared from hearts of 1–2 day old mouse pups as described previously[1]. Arterial myocytes were prepared from freshly dissected basilar, middle and posterior cerebral arteries as described in detail elsewhere[2].

### *Cav1.2 and CaM constructs and their expression in tSA cells*

Plasmids encoding the pore forming subunit of the wild type (WT) dihydropyridine-sensitive, voltage-gated $Ca^{2+}$ channel pore-forming and accessory subunits (rabbit and mouse Cav1.2 ($\alpha_{1c}$), Cav-$\beta_3$ and Cav-$\alpha_2\delta_1$) were provided by Dr. Diane Lipscombe. We generated the rabbit homolog of the human Timothy syndrome Cav1.2 (G436R, Rabbit; G406R Human)[3]. The Cav1.2 mutant with a stop codon at amino acid 1670 (Cav1.2Δ1670X) and calmodulin (CaM) were kindly provided by Dr. David T. Yue. Plasmids for the enhanced green fluorescent protein (EGFP) and the tag-RFP® (tRFP) were purchased from Invitrogen and Evrogen, respectively. tRFP and EGFP were fused to the C-tail of Cav1.2 and Cav1.2-TS, yielding Cav1.2-TS-tRFP, Cav1.2-TS-EGFP, Cav1.2-tRFP, and Cav1.2-EGFP. For experiments examining CaM association with the IQ domain in the C-terminal of WT Cav1.2 via FRET, we used a Cav1.2 channels with a C-tail truncated just after the IQ site without stop codon and tagged with EGFP as described previously[4]. The CaM-tRFP construct was generated by PCR amplification of rat CaM cDNA followed by fusion to the carboxyl terminus of the tRFP. tsA-201 cells were cultured in Dulbecco's Modified Eagle Medium supplemented with 10% fetal bovine serum, L-glutamine (2 mmol/L), and a 1% streptomycin and penicillin solution. Cells were transiently transfected with using JetPEI. Successfully transfected cells were identified on the basis of EGFP or tRFP fluorescence.

### *Inducible PKCα translocation*

A rapamycin-induced PKCα translocation system similar to the one developed by Liberles *et al*[5] and Suh *et al*[6] was developed for some of the experiments included in this study. The system requires the expression of a FKBP12-rapamycin-binding element (FRB) that is anchored to the plasma membrane via the myristoylation and palmitoylation modification sequence $Lyn_{11}$. It also expresses PKCα fused to the enhanced green fluorescent protein and a FK506 binding protein. Application of rapamycin promoted heterodimerization of protein domains from FKBP-PKCα-EGFP and the membrane anchored FRB. This recruited FKBP-PKCα-EGFP to the membrane from the cytosol upon addition of rapamycin.

The membrane anchored Lyn11-FRB and CFP-FKBP vectors were obtained from Agilent Technologies. Mouse PKCα cDNA (kindly provided by Dr. John Exton) was amplified and fused to the carboxyl terminus of EGFP in pEGFP-C2 vector. Then, FKBP was PCR amplified from CFP-FKBP vector and inserted in the middle of EGFP and PKCα within the correct reading frame. Then EGFP-FKBP-PKCα fragment was PCR amplified and sub-cloned downstream of IRES in pIRES vector. Finally, membrane-anchored Lyn11-FRB was PCR amplified from Lyn11-FRB vector and inserted upstream of IRES to obtain the final Lyn11-FRB-pIRES-EGFP-FKBP-

PKCα construct. We transfected tsA-201 cells with this construct and the calcium channel subunits using JetPEI. For those experiments involving neonatal myocytes, an adenovirus vector delivering Lyn11-FRB-pIRES -EGFP-FKBP-PKCα was generated. To do this, the 4.2 kb Lyn11-FRB-IRES-EGFP-FKBP-PKCα fragment was amplified and subcloned into pENTR 1A (Invitrogen) vector using Quick PCR Cloning Kit (BPS Bioscience). Then the target sequence was recombined into adenoviral expression vector pAd/CMV/V5-DEST. The adenoviral expression clone was digested with Pac I and purified using phenol-chloroform extraction followed by ethanol precipitation. We used 1 μg of Pac I-digested plasmid DNA to transfect 293A producer cell line using jetPEI DNA transfection reagent. Crude viral lysate was harvested 2 days after transfection. The adenoviral construct was amplified by infecting 293A producer cells using 100 μl crude lysate. Virus lysate was harvested 2 days later and stored in -80°C. A 500 μl of virus lysate was used to transduce mouse neonatal myocytes. Transgene expression was detected 2 days after infection.

### *Electrophysiology*

Membrane potential was controlled using the whole-cell configuration of the patch-clamp technique using a HEKA EPC10 amplifier. Cells were patched in the presence of a solution with the following constituents (mmol/L): 140 NaCl, 5 $CsCl_2$, 2 $CaCl_2$, 1 $MgCl_2$, 10 glucose, 10 HEPES adjusted to pH 7.4. Once a GΩ seal was formed and successful conversion to whole-cell patch-clamp configuration was achieved, this solution was exchanged for a solution containing a similar composition except that it had no $Na^+$, $CaCl_2$ was 20 mmol/L and NMDG concentration was 120 mmol/L. Pipettes for whole-cell patch-clamp experiments were filled with a solution containing (in mmol/L): 87 Cs-aspartate, 20 CsCl, 1 $MgCl_2$, 5 MgATP, 10 EGTA, 10 HEPES, and 0.2 fluo-5F or rhod-2 adjusted to pH 7.2 with CsOH. All experiments were performed at room temperature (22-25°C).

We recorded L-type $Ca^{2+}$ channel currents from cell-attached patches from neonatal ventricular myocytes and tsA-201 cells expressing WT Cav1.2 and Cav1.2-TS channels. The patch pipette solution contained 20 mmol/L $Ca^{2+}$ (charge carrier), 10 μmol/L tetrodotoxin (TTX), 130 mmol/L $TEA^+$ and no $Na^+$ or $K^+$ to eliminate $Na^+$ and $K^+$ channel currents (pH = 7.2). The L-type $Ca^{2+}$ channel opener BayK-8644 (500 nmol/L) was included in the pipette solution to increase the mean open time and open probability ($P_o$) of these channels. With this solution, patch pipette resistances ranged from 4-5 MΩ. Currents were recorded while cells were exposed to a solution containing 145 mmol/L KCl, 10 mmol/L HEPES, and 10 mmol/L NaCl (pH = 7.4). L-type $Ca^{2+}$ channel currents were evoked by a 2 s step depolarization to -30 mV from the holding potential of -80 mV. In some experiments, a modified patch-pipette including the L-type $Ca^{2+}$ channel blocker nifedipine (10 μmol/L) was used. Inward $Ca^{2+}$ currents were never recorded in the presence of nifedipine, indicating that L-type $Ca^{2+}$ channels produced the currents recorded at -30 mV. Membrane currents were recorded and analyzed using pCLAMP 9 software.

### *TIRF and confocal microscopy*

$Ca^{2+}$ sparklet images were acquired using a through-the-lens TIRF microscope built around an inverted Olympus IX-71 microscope equipped with an Olympus PlanApo (60X, NA = 1.45) oil-immersion lens and an Andor iXON 597 EMCCD camera. Images were acquired at 100-200 Hz using TILL Image software. To monitor $[Ca^{2+}]_i$, cells were loaded with the calcium indicators fluo-5F or rhod-2. Rhod-2 was used in all experiments in which the enhanced green fluorescent protein was expressed. Excitation of fluo-5F and rhod-2 was achieved with 491 or 563 nm solid-state lasers. Excitation and emission light was separated with the appropriate set of filters. $Ca^{2+}$

sparklets were recorded in cells exposed to 1 μmol/L thapsigargin to eliminate $Ca^{2+}$ release from intracellular stores.

Background-subtracted fluorescence signals were converted to concentration units using the "$F_{max}$" equation[7]:

$$\left[Ca^{2+}\right] = K_d \frac{F/F_{\max} - 1/R_f}{1 - F/F_{\max}}$$

Where F is fluorescence, $F_{max}$ is the fluorescence intensity of fluo-5F or rhod-2 in the presence of a saturating free $Ca^{2+}$ concentration, $K_d$ is the dissociation constant of the fluorescence indicator used (fluo-5F = 1280 nmol/L; rhod-2 = 100 nmol/L), and $R_f$ (fluo-5F = 280; rhod-2 = 150) is this indicator's $F_{max}/F_{min}$. $F_{min}$ is the fluorescence intensity of fluo-5F or rhod-2 in a solution where the $Ca^{2+}$ concentration is 0. $K_d$ and $R_f$ values for Fluo-5F and rhod-2 were determined *in vitro* using standard methods[8]. $F_{max}$ was determined at the end of experiments by exposing cells to a solution to which the $Ca^{2+}$ ionophore ionomycin (10 μmol/L) and 20 mmol/L external $Ca^{2+}$ had been added.

$Ca^{2+}$ sparklets were detected and defined for analysis using an automated algorithm written in IDL language. $Ca^{2+}$ sparklets had an amplitude equal to or larger than the mean basal $[Ca^{2+}]_i$ plus three times its standard deviation. For a $[Ca^{2+}]_i$ elevation to be considered a sparklet, a grid of 3 X 3 contiguous pixels had a $[Ca^{2+}]_i$ value at or above the amplitude threshold. These detection criteria for $Ca^{2+}$ sparklets are similar to those used by other investigators[9-11].

We determined that $Ca^{2+}$ sparklets were produced by $Ca^{2+}$ influx via L-type $Ca^{2+}$ channels using multiple strategies. First, sparklet activity in smooth muscle cells, neonatal ventricular myocytes, and tsA-201 cells transfected with Cav1.2 was rapidly eliminated by the application of the L-type $Ca^{2+}$ channel inhibitor nifedipine (10 μmol/L) or by superfusion of a $Ca^{2+}$-free external solution (*data not shown*). Second, as reported previously[8], $Ca^{2+}$ sparklets were never observed in untransfected tsA-201 cells. Third, $Ca^{2+}$ sparklets in arterial and neonatal ventricular myocytes have the same amplitude of quantal event, activity, and pharmacology (e.g. insensitive to 1 μmol/L thapsigargin, eliminated by 10 μmol/L nifedipine) as $Ca^{2+}$ sparklets in tsA-201 cells expressing Cav1.2 channels[8, 16].

By simultaneously recording single $Ca^{2+}$ channel currents and $Ca^{2+}$ sparklets in arterial myocytes, we recently reported that at -70 mV and with 20 mmol/L external $Ca^{2+}$ a single $Ca^{2+}$ channel current of ≈0.7 pA produced a $Ca^{2+}$ sparklet of ≈40 nmol/L[12]. As shown in previous studies[2, 12], histograms from all $[Ca^{2+}]_i$ records obtained from arterial myocytes had multiple, clearly separated peaks and could be fit with the following multi Gaussian function:

$$N = \sum_{j=1}^{n} a_j * \exp\left[-\frac{([Ca^{2+}]_i - jq)^2}{2jb}\right]$$

Where a and b are constants and $[Ca^{2+}]_i$ and *q* are intracellular $Ca^{2+}$ and the quantal unit of $Ca^{2+}$ influx, respectively. Using this analysis, and consistent with our previous studies, we obtained a *q* value of 38 nmol/L in the histogram, a value that is similar to that obtained previously (see above). This analysis provides further support to the hypothesis that $Ca^{2+}$ sparklets are quantal in nature and that the size of $Ca^{2+}$ sparklet depends on the number of quanta activated.

Quicktime movie tutorials of this analysis are available in our lab webpage (http://web.mac.com/fernando_santana/Lab_website/Sparklet_tutorials.html).

We determined the number of $Ca^{2+}$ sparklet sites with coupled gating events per cell as follows. First, we identified $Ca^{2+}$ sparklet sites in each cell as described above. Next, we analyzed the $Ca^{2+}$ sparklets records from these sites using the coupled Markov model described below to determine the coupling co-efficient of the $Ca^{2+}$ channels underlying these sparklets. We created bar plots of the number of sites per cell with coupling coefficients > 0. Because $Ca^{2+}$ sparklets were recorded using TIRF, this analysis was limited to the portion of the cell within the evanescent field (typically 100-400 $\mu m^2$).

Confocal images were obtained using the 60X lens (NA = 1.4 or 1.2) of an inverted microscope coupled to a BioRad Radiance 2100 confocal system. The all-points histograms shown in Figure 1 and 2 were fitted using a least-squares routine with a multi-component Gaussian function using Graphpad Prism v5 (San Diego, CA)

### *Coupled Markov chain model*

Membrane currents and time courses of $[Ca^{2+}]_i$ from $Ca^{2+}$ sparklet sites were analyzed using a binary coupled Markov chain model originally described by Chung and Kennedy[13] to simulate and fit independent records of partially coupled channels. The program was written in Matlab® language. Channel openings were identified using a half-amplitude protocol, with the quantal level for a unitary event set at 0.50 pA for currents and 38 nmol/L for $Ca^{2+}$ sparklets[12]. The activity of Cav1.2 channels was modeled as a first order, discrete Markov chain, and the Markovian transition matrix was estimated from the current and sparklet records and their corresponding channel opening time courses using the built-in Hidden Markov parameter estimation function in Matlab®. The estimated transition matrix was modeled as a partially coupled Markov chain where a dimensionless parameter (κ) is the coupling coefficient between fully uncoupled and fully coupled cases. In addition to the coupling coefficient (κ), the model has two additional parameters: the channel open-to-open probability (ρ) and the channel closed-to-closed probability (ς), and together they fully describe the contribution from the fully uncoupled case to the transition matrix. For each record, the optimum set of parameters (κ, ρ, ς) for the partially coupled Markov chain model was fitted using a gradient descent algorithm.

The utility of this model is that it is a “lumped” model, where the channels switch between the binary observable states of either “open” or “closed,” and therefore, instead of trying to deduce the gating kinetics of multiple channels, which involves many free parameters, our model has only three free parameters, including the coupling coefficient. It does not completely describe the actual kinetics of the channel and consequently the transition probabilities obtained from this lumped model are not interpreted as rate constants.

### *FRET imaging*

For these experiments, we used tsA-201 cells transfected with Cav1.2-EGFP and CaM-tRFP, Cav1.2-TS-EGFP and CaM-tRFP, Cav1.2-EGFP and Cav1.2-tRFP, or Cav1.2-TS-EGFP and Cav1.2-TS-tRFP as described above. FRET was determined using a confocal microscope using approaches similar to those described by Tadross *et al*[14]. Cells were imaged using a Nikon swept field confocal system coupled to a Nikon TE300 inverted microscope equipped with a Nikon 60x lens (NA = 1.2) and using a slit aperture of 60 µm (maximum apperture). This optical configuration has been shown to produce robust sub-cellular FRET imaging[14]. EGFP and tRFP

were excited using 488 and 563 nm light, respectively and appropriate dichroic (500/543 nm long-pass) and emission (dual 535/30 nm and 610/40) filters. Images were acquired with a Cascade EMCCD camera.

The efficiency of FRET between EGFP and tRFP was determined using the donor de-quenching method as described elsewhere [4, 15]. Briefly, images of EGFP-tagged proteins (donor) were collected before and after the PKC activator PDBu (500 nmol/L) or the CaM inhibitor W7 (100 µmol/L) and after approximately complete photobleaching of tRFP-tagged (acceptor) proteins. During analysis, we generated fluorescence intensity profiles (1 µm wide) of portions of the images that included the surface membrane and cytosol of each cell analyzed before and after photo-bleaching tRFP (i.e. acceptor). FRET was reflected by an increase in EGFP fluorescence intensity following tRFP bleaching. The effective FRET was calculated using the following equation: $E_{EFF} = 1 - (F_{DA}/F_D)$, where $E_{EFF}$ is the effective FRET, $F_{DA}$ is the fluorescence intensity of EGFP before acceptor photo-bleaching, and $F_D$ is the fluorescence intensity of EGFP after tRFP photo-bleaching with 563 nm light[16].

### *Statistics*

Data are presented as mean ± SEM. Two-sample comparisons were made using a students' T-test or a Wilcoxon signed-rank test. A *p* value of less than 0.05 was considered significant. The asterisk (*) symbol is used in the figures to illustrate a significant difference between groups.

### *Supporting references*


**1.** Devic E, Xiang Y, Gould D, Kobilka B. Beta-adrenergic receptor subtype-specific signaling in cardiac myocytes from beta(1) and beta(2) adrenoceptor knockout mice. *Mol Pharmacol.* 2001;60:577-583.

**2.** Navedo MF, Amberg GC, Nieves M, Molkentin JD, Santana LF. Mechanisms Underlying Heterogeneous $Ca^{2+}$ Sparklet Activity in Arterial Smooth Muscle. *Journal of General Physiology.* 2006;127:611-622.

**3.** Erxleben C, Liao Y, Gentile S, Chin D, Gomez-Alegria C, Mori Y, Birnbaumer L, Armstrong DL. Cyclosporin and Timothy syndrome increase mode 2 gating of CaV1.2 calcium channels through aberrant phosphorylation of S6 helices. *Proc Natl Acad Sci U S A.* 2006;103:3932-3937.

**4.** Erickson MG, Alseikhan BA, Peterson BZ, Yue DT. Preassociation of calmodulin with voltage-gated $Ca^{2+}$ channels revealed by FRET in single living cells. *Neuron.* 2001;31:973-985.

**5.** Liberles SD, Diver ST, Austin DJ, Schreiber SL. Inducible gene expression and protein translocation using nontoxic ligands identified by a mammalian three-hybrid screen. *Proc Natl Acad Sci U S A.* 1997;94:7825-7830.

**6.** Suh BC, Inoue T, Meyer T, Hille B. Rapid chemically induced changes of PtdIns(4,5)P2 gate KCNQ ion channels. *Science.* 2006;314:1454-1457.

**7.** Maravall M, Mainen ZF, Sabatini BL, Svoboda K. Estimating intracellular calcium concentrations and buffering without wavelength ratioing. *Biophys J.* 2000;78:2655-2667.

**8.** Woodruff ML, Sampath AP, Matthews HR, Krasnoperova NV, Lem J, Fain GL. Measurement of cytoplasmic calcium concentration in the rods of wild-type and transducin knock-out mice. *J Physiol.* 2002;542:843-854.

**9.** Cheng H, Song LS, Shirokova N, Gonzalez A, Lakatta EG, Rios E, Stern MD. Amplitude distribution of calcium sparks in confocal images: theory and studies with an automatic detection method. *Biophys J.* 1999;76:606-617.
**10.** Demuro A, Parker I. Imaging the activity and localization of single voltage-gated $Ca^{2+}$ channels by total internal reflection fluorescence microscopy. *Biophys J.* 2004;86:3250-3259.
**11.** Demuro A, Parker I. "Optical patch-clamping": single-channel recording by imaging $Ca^{2+}$ flux through individual muscle acetylcholine receptor channels. *J Gen Physiol.* 2005;126:179-192.
**12.** Navedo MF, Amberg G, Votaw SV, Santana LF. Constitutively active L-type $Ca^{2+}$ channels. *Proc Natl Acad Sci U S A.* 2005;102:11112-11117.
**13.** Chung SH, Kennedy RA. Coupled Markov chain model: characterization of membrane channel currents with multiple conductance sublevels as partially coupled elementary pores. *Math Biosci.* 1996;133:111-137.
**14.** Tadross MR, Park SA, Veeramani B, Yue DT. Robust approaches to quantitative ratiometric FRET imaging of CFP/YFP fluorophores under confocal microscopy. *J Microsc.* 2009;233:192-204.
**15.** Day RN, Voss TC, Enwright JF, 3rd, Booker CF, Periasamy A, Schaufele F. Imaging the localized protein interactions between Pit-1 and the CCAAT/enhancer binding protein alpha in the living pituitary cell nucleus. *Mol Endocrinol.* 2003;17:333-345.
**16.** Selvin PR. Fluorescence resonance energy transfer. *Methods in enzymology.* 1995;246:300-334.